The UTB Electron-Hole Bilayer LED

Florian Mema
Bachelor Assignment
University of Twente
Faculty of Electrical Engineering, Mathematics and Computer Sciences
Enschede, the Netherlands

Abstract—Electrostatic doping is emerging as an alternative for nanometer-scale or ultrathin-body (UTB) semiconductor devices, given the constraints of chemical doping in UTB layers. This paper aims to perform a technology computer aided design (TCAD) simulation study on a new form of electrostatic doping in a light-emitting diode (LED): the electron-hole bilayer LED. As the name suggests an electron-hole bilayer has formed, in a vertical p-n junction configuration, by means of work-function induced doping and application of bias voltage on the gates. As has been reported before, this electron-hole bilayer concept can also be used in other types of devices, such as tunnel FETs.

Keywords— carrier concentrations, doping, electron-hole bilayer (EHB), metal work-function, quantum model, supercoupling, ultrathin-body (UTB)

I. INTRODUCTION

Chemical doping is showing limitations in nanometer-scale ultrathin-body (UTB) semiconductor devices, that is why alternatives are being researched that can overcome the constraints. Electrostatic doping (ED) [1] is one of the methods being broadly investigated as an option that can provide high electron or hole densities in semiconductors. ED is a technique in which charge carriers (electrons or holes) are induced in a semiconductor material as a result of its band alignment near its interface with another (semi)conducting material. In the ED approach, the relative separation, between the Fermi level and the semiconductor energy bands, that governs the active doping concentration, is controlled by the potential and the work-function of the electrode adjacent to the semiconductor body rather than by the chemical impurities as in conventional doping. [1]

In this paper, a device concept is discussed based on the work of Prunnila and Ahopelto [2],[3]. In this device concept, as shown in fig. 1, a semiconductor is layered between two insulating layers (*e.g.*, oxide) in a vertical configuration and a voltage is applied on the metal gates. The basic idea behind the device is that by applying reverse bias on the gates, an electrostatic field will induce electron and hole densities in the semiconductor structure, forming *i.e.* an electron-hole bilayer (EHB) with a depleted region in the middle and high carrier concentrations at the front (electrons) and back (holes) side of the semiconductor. A forward bias will cause the carriers to move towards the depleted region and recombine. As a result of radiative recombination, a photon is emitted for every electron-hole pair recombined, thus producing light of wavelength corresponding to the material choice.

Throughout this paper, reverse and forward bias are defined as the bias configurations on the gates that results in high and low carrier densities formation respectively on the semiconductor sides, with holes at the back and electrons at the front.

The process repeats itself to produce a continuous source of light such as in a light-emitting diode (LED).

Figure 1. Schematic cross section of the EHB device concept. Hole region formation at the back, and electron region at the front of the device (left). Energy band diagram perpendicular to the gates along the red dashed line (right) [1]

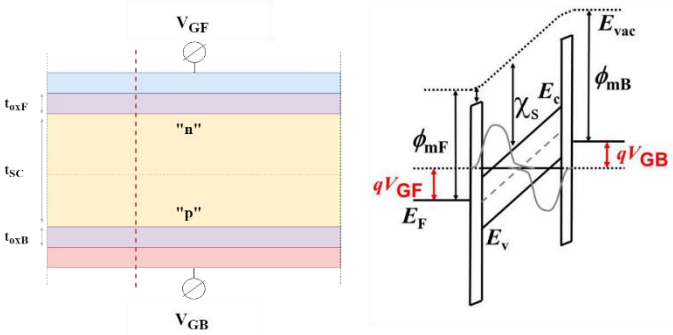

In [4] however, Hueting *et al.* propose to use two different work-function metals in the gates to induce charge carriers of different polarities in the semiconductor. The gate work-functions are determined by the electron affinity of the semiconductor (χ_{SC}), as well as its bandgap (E_{gsc}). Applying this work-function-induced doping concept to the above device results in carrier generation process through the metal work-function induction with no bias applied on the gates.

For light applications, direct bandgap semiconductors are preferred compared to indirect bandgap ones in view of efficiency. For radiative recombination to take place, in direct bandgap direct transitions between the valence and conduction band energies are possible for which no phonons are required. While in indirect bandgap ones, this would require the involvement of a phonon, reducing the

probability of recombination happening in a certain timespan and therefore slowing the process down. [5] Direct bandgap semiconductors commonly used in LED fabrication include group III-V material compounds such as GaN, GaAs, InAs, InN, etc. [6]

The oxide used is hafnium-dioxide (HfO_2), a commonly used insulator in metal-oxide semiconductor devices.

With the device concept and basic configuration presented above, this paper aims to answer the following questions:

- Will the proposed EHB-LED work? If so, how and for what boundary conditions?
- What will be the effect of different device configurations (work-functions choice, layer thickness, etc.) on the performance of the EHB-LED?
- Can this EHB-LED compare to its conventional counterparts and what (other) possible applications are there for this EHB principle?

II. Method

Based on [4], the choice of work-functions of the gates is dependent on semiconductor characteristics, as in:

$$\phi_{\mathrm{m,F}} < \chi_{\mathrm{SC}} + \frac{E_{\mathrm{gsc}}}{2} < \phi_{\mathrm{m,B}}\,, \qquad (1)$$

in which $\phi_{\mathrm{m,B}}$ and $\phi_{\mathrm{m,F}}$ are the work-functions of the back and front gate metals, respectively.

Initial simulations in this paper will be conducted for indium-arsenide (InAs). With a wavelength of $2.97\mu m$, it emits light in the infrared region of the spectrum, but its small bandgap means less energy is required in promoting a valence electron to the conduction band, thus being able to move freely within the crystal lattice and serve as a charge carrier.

For InAs, the values in (1) at room temperature (300K) correspond to $\chi_{\mathrm{SC}} = 5.0284eV$, and $E_{\mathrm{g}} = 0.4170eV$ [6], resulting in metal work-functions for the gates of

$$\phi_{\mathrm{m,F}} < 5.2369eV, \phi_{\mathrm{m,B}} > 5.2369eV. \quad (2)$$

The difference between both work-functions is suggested at ~0.5eV [4]. This led to the work-function choice of $\phi_{\mathrm{m,F}} = 4.82eV$, and $\phi_{\mathrm{m,B}} = 5.65eV$, corresponding to gold (Au) and platinum (Pt) [12].

The thickness chosen for both oxide layers is 4nm. Generally, reducing the oxide thickness could result in high leakage currents, however in the simulations this is not modeled and is not accounted for. A thin oxide layer also allows for a lower threshold voltage hence better electrostatic coupling [7].

2-D TCAD simulations applying both semiclassical (Poisson) and Quantum Mechanical (density-gradient model) approaches were performed on Synopsys Sentaurus (v.2016.03) [8] on a device model provided by the University of Twente with the following device parameters (table 1).

Table 1. Parameter values for the simulations

t_{oxB}	4nm
t_{oxF}	4nm
t_{SC}	10-80nm
χ_{SC}	5.0284eV
E_{g}	0.4170eV
B_{Rad}	$1.1\cdot10^{-10}$ cm^3s^{-1}
τ_{SRH}	$1\cdot10^{-9}$ s
$n_{i_{InAs}}$	10^{15} cm^3

Where t_{oxB} and t_{oxF} are the back and front oxide thicknesses respectively, t_{SC} is the semiconductor thickness, χ_{SC} is the semiconductor electron affinity, E_g is the semiconductor bandgap, B_{Rad} is semiconductor radiative recombination coefficient, τ_{SRH} is the semiconductor SRH recombination lifetime, and n_i is the semiconductor intristic carrier concentration.

Models used [8]:

EffectiveIntrinsicDensity(NoBandGapNarrowing)

Recombination(SRH Auger Radiative)

Mobility(DopingDependence

eHighFieldSat(GradQuasiFermi)

hHighFieldSat(GradQuasiFermi))

Fermi

Simulations were initially performed in steady state, in order to determine the optimal values for the device thickness, and bias choice. Further simulations with varied metal work-functions illustrate the effects of their choice on the carrier concentrations. Transient simulations with the optimized device will determine the theoretical potential of the concept and its feasibility.

III. Results

Figures 2 A and B show the simulation results in steady state ($V_{\mathrm{GB}} = 0.0V, V_{\mathrm{GF}} = 0.0V$). Electron concentrations are formed at the front side of the semiconductor, and hole concentrations at the back, induced by the work-functions of the gate metals. There appears to be no depletion region due to the small scale of the device, but it becomes noticeable as the semiconductor width increases beyond the UTB scale (30-80nm). For a table of values refer to Appendix A.

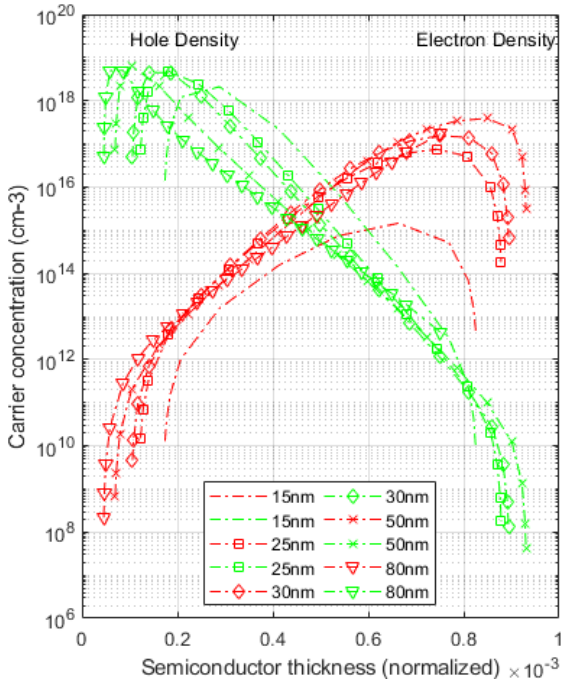

Figure 2A. Carrier concentration for different semiconductor thicknesses (normalized) at thermal equilibrium (green-hole concentration, red-electron concentration). Refer to Appendix A for more data.

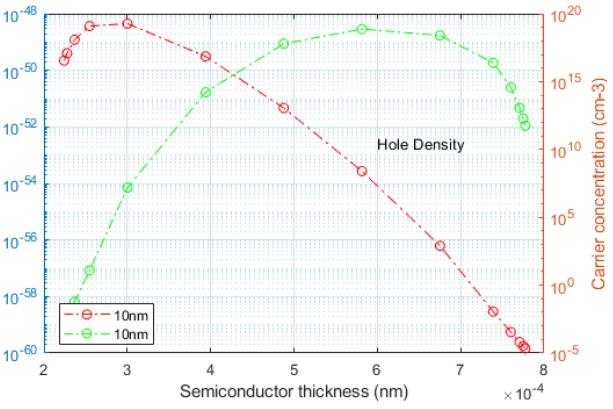

Figure 2B. Carrier concentration for 10nm semiconductor thickness at thermal equilibrium (green-hole concentration, red-electron concentration). At 10nm simulations show the effect of supercoupling on the device, as one carrier type dominates.

Due to the small distance between the gates (tens of nanometers), the effect of both gates on each charge carrier profile is noticeable. The choice of adopting symmetric work-functions would yield more or less equal carrier concentration profiles. As can be seen though that is not the case unless the distance increases. The effect is more noticeable for semiconductor thicknesses of <10nm (fig. 2B), when supercoupling [9] comes into play. For a critical semiconductor thickness, only one type of carriers becomes prominent irrespective of the applied bias on the gates. In [9], Cristoloveanu *et al*. discuss the effects of supercoupling in UTB silicon films, and observe the critical thickness for that semiconductor also at ~10nm, as explained in [10] where this critical thickness has been analytically modelled and introduced.

For light emitting purposes, radiative recombination is required, and increasing the carrier concentrations will result in a higher radiative recombination rate [11]. However, Shockley-Read-Hall (SRH) recombination becomes important for low carrier concentrations and $n = p$ [11]. SRH recombination occurs via traps which reduces the efficiency, and therefore it is preferred to minimize it. For $n \neq p$, and high concentrations, which is a result of what was previously discussed, the SRH recombination rate would decrease, increasing the efficiency of the LED.

Results show (fig. 3) that an optimal carrier concentration can be achieved in the region between 20nm and 50nm. Below 20nm, the quantum mechanical and supercoupling effects on the semiconductor structure become too high.

The simulations were run using quantum mechanical models to improve accuracy. To illustrate the quantum mechanical effects, in figure 3 a comparison between the results with and without a quantum model in the simulation can be seen.

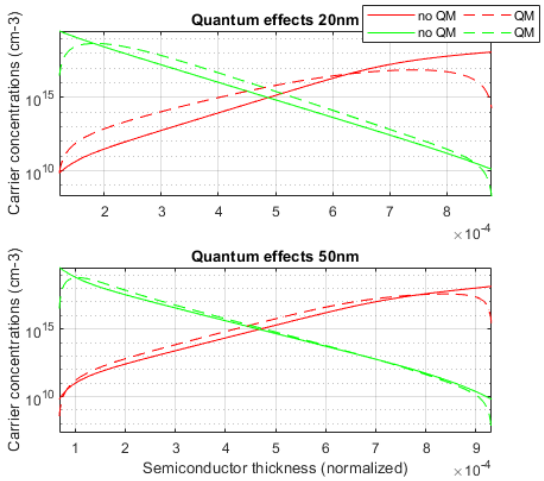

Figure 3. Simulation results with and without the quantum models (red – electron density, green – hole density). For larger semiconductor thicknesses the effect becomes less relevant and the lines start to align

Proceeding with the simulations, a semiconductor thickness of 25nm is chosen as reference. It resulted in carrier concentrations of $n_F = 7.4721x10^{16}$ and $p_B = 4.8203x10^{18}$ at $0V$ bias on the gates. In fig. 4 A and B, results are shown for different bias configurations applied on the gates. As seen earlier, when no bias is applied on the gates the concentrations are already high, due to the work-function induced carriers. To increase these concentrations, negative bias can be applied on the bottom gate and positive bias on the top. However, in transient simulations a smaller voltage swing is initially going to be considered (between $0V$ and $\pm 0.5V$ instead of $-0.5V$ and $+0.5V$).

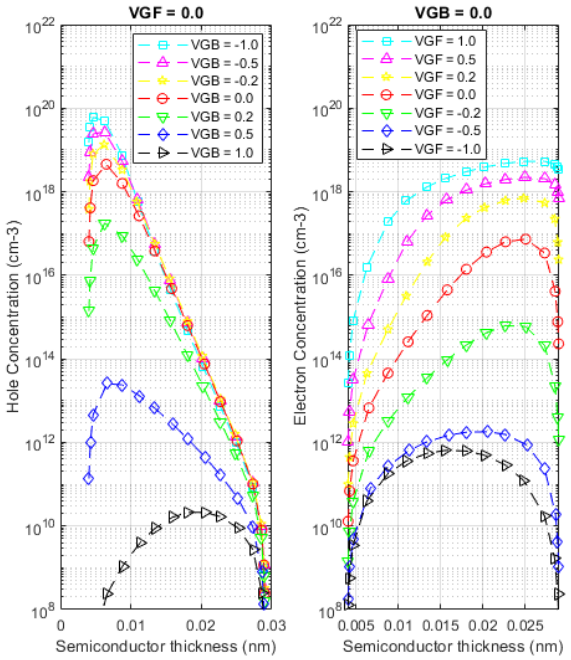

Figure 4A. Simulation results when keeping one gate at 0.0V while varying the other. Forward voltages of higher than 0.5V in the back gate, and lower than -0.5V in the front gate will reduce the carrier densities below the semiconductor intrinsic value. For a table of values refer to Appendix B

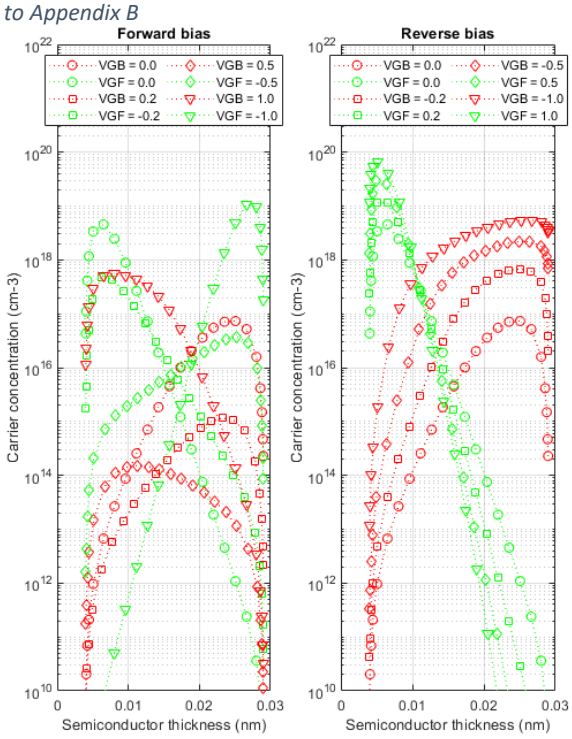

Figure 4B. Simulation results for simultaneously applying a potential on both gates; Forward bias (left) and Reverse bias (right), with electron concentration in red and hole concentration in green. Forward bias of higher than |0.5|V will cause the gates to reverse dopant concentrations (there will be hole concentrations in the front and electrons in the back)

Forward bias reduces the carrier concentrations, forcing them towards the center of the semiconductor body. However, applying a bias higher than 0.5V on the back gate, and lower than -0.5V at the front gate reverses the carrier concentrations, resulting in an electron density formation in the back side, and holes at the front side of the semiconductor. In transient simulations, this situation is not preferred.

In order to obtain the highest recombination rate, the majority of the carriers should be guided towards the center of the semiconductor body without reversing the band structure. This can be achieved at a forward bias of $V_{\mathrm{GB}} \approx 0.5V$ and $V_{\mathrm{GF}} \approx -0.5V$.

Another important factor is the thermal carrier generation time. To generate a concentration of n_0 for one type of carriers (electrons chosen for calculation), the total time needed T is:

$$T = \frac{n_{\mathrm{o}}}{\frac{n_{\mathrm{i}}}{2\tau_{\mathrm{SRH}}} + B_{\mathrm{Rad}} n_{\mathrm{i}}^2} \qquad (3)$$

Where n_{i} and n_{o} are the intrinsic and final (desired) carrier density, τ_{SRH} is the SRH recombination lifetime, and B_{Rad} the radiative recombination coefficient. The formula indicates that the process does not depend on the bias applied. For a derivation of (3) refer to Appendix C.

Substituting for InAs and a final carrier density of $10^{18}\ cm^{-3}$ results in $1.99\mu s$. A higher switching frequency for the bias would not allow for the carrier concentrations to reach this settling point.

This can be seen in figure 5 for the electron density at different switching frequencies for the bias voltage.

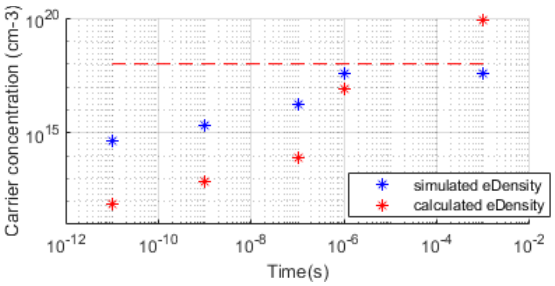

Figure 5. Calculated (red) and simulated (blue) results for carrier concentrations at different bias switching times. The formula in (5) gives a linear trend for n_o, but as can be seen after a certain time (~2 μs) the electron concentration levels out at the expected final value (red interrupted line = $10^{18} cm^{-3}$). Therefore, it is limited by the values obtained in steady state simulations, and allowing for a longer time for carrier densities to form will not result in higher densities.

Using the nominal values obtained for the bias level ($V_{\mathrm{GB}} = 0.5V, V_{\mathrm{GF}} = -0.5V$) and semiconductor thickness (25nm), results on transient simulations of the device are shown in figure 6. The initial bias on the gates is set to forward, such that the electron or hole concentrations in the semiconductor front and back reach the intrinsic value for InAs ($10^{15}\ cm^{-3}$), *i.e.* the semiconductor is 'undoped'. The voltage swings every $10\mu s$ between $\pm 0.5V$ and 0V with a $10\mu s$ transition time.

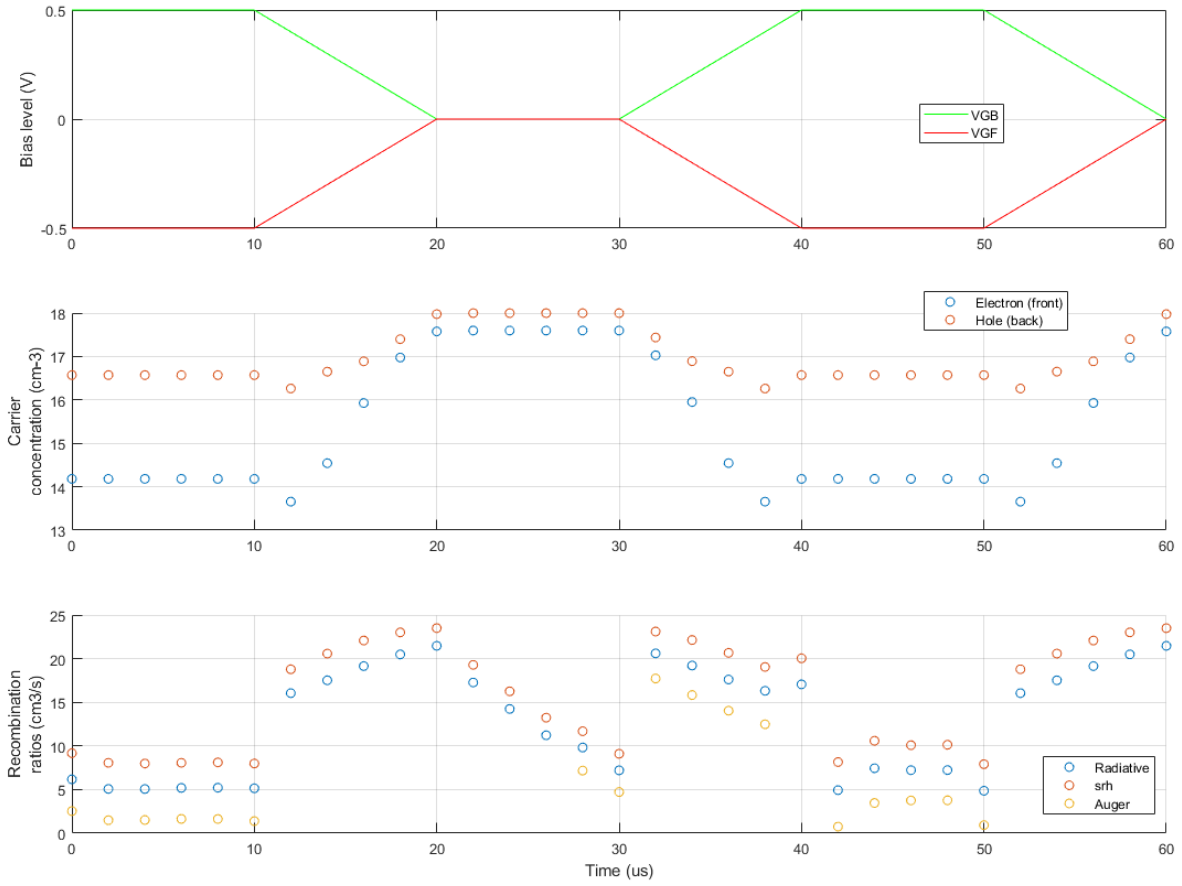

Figure 6. Transient simulation on the device. Top graph shows the applied signal on the front and back gates at each time instant. Middle graph shows the maximum carrier concentration in the front and back corresponding to each time instant. Bottom graph shows the recombination rates by the carrier concentrations at that time instant. For a table of values refer to Appendix D.

IV. Discussion

The calculated radiative recombination rate is [10]

$$R_{\mathrm{Rad}} = B_{\mathrm{Rad}}(pn - n_{\mathrm{i}}^2), \qquad (4)$$

where B_{Rad} is the recombination coefficient at 300K, p and n are the carrier concentrations.

Substituting for InAs ($n_{\mathrm{i}} = 1x10^{15} cm^{-3}$, $B_{\mathrm{Rad}} = 1.1x10^{-10}\, cm^3/_s$) and the carrier concentrations deducted from the steady state simulations at $V_{\mathrm{GB}} = 0.0V$, $V_{\mathrm{GF}} = 0.0V$, the expected radiative recombination rate is

$$R_{\mathrm{Rad}} = 3.96x10^{24}\, cm^{-3}/_s \qquad (5)$$

From the simulation results the value $2.9x10^{21}\, cm^{-3}/_s$ was obtained in the case of bias switch between 0 and 0.5V in the back gate and 0 and -0.5V in the front gate.

The simulations were also run with a swing of $-0.5V$ to $+0.5V$ in the back gate and $+0.5V$ to $-0.5V$ in the front gate in order to have higher concentrations before recombination, and a radiative recombination rate of $8.2x10^{23}\, cm^{-3}/_s$ was obtained. A table of values is included for this case also in Appendix D. As expected, the radiative recombination increased when the carrier concentrations were increased, and the SRH recombination rate decreased.

Calculating the internal quantum efficiency (IQE) using:

$$IQE = \frac{R_{\mathrm{Rad}}}{R_{\mathrm{Rad}} + R_{\mathrm{SRH}} + R_{\mathrm{Auger}}} \qquad (6)$$

results in 0.9% efficiency in the case when no bias induced carrier are present, and 69.1% when bias is applied to increase the carrier concentrations.

The efficiency can be improved by increasing the carrier concentrations; there are three factors that can be tweaked to achieve this: (1) increase the difference between work-function values, (2) apply reverse bias on the gates, (3) reduce semiconductor thickness.

In fig. 7 the first case is illustrated with a simulation for a small difference increase of 0.2eV in work-functions ($\phi_{\mathrm{m,F}} = 4.72eV$, and $\phi_{\mathrm{m,B}} = 5.75eV$). However, the bottom gate work-function does not correspond to any available value for a metal work-function, and was considered only to show that theoretically an increase in the difference between work-functions does result in higher carrier concentrations.

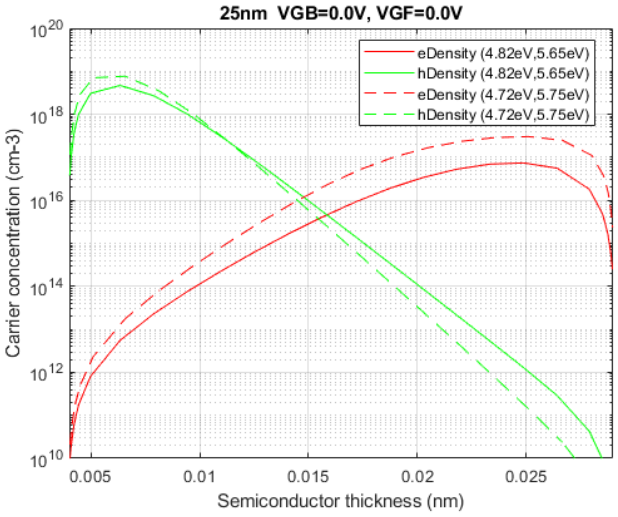

Figure 7. Carrier concentrations for different gate work-functions. Increasing the difference between the gate workfunctions increases the carrier concentrations. For a table of values refer to Appendix A

The second case was shown in the transient simulations with a larger swing where bias was applied in order to increase the carrier concentrations prior to recombination. The third case was discussed at the start, where reducing the semiconductor thickness would result in the supercoupling effect yielding lower charge carrier concentrations rather than the opposite.

Another important factor is the electric field in the vertical interface of the device. Gupta *et al.* [1] concluded that for higher effectiveness of the EHB concept, a higher electric field is required. However, the breakdown values for the materials should not be exceeded in order for the device to function properly. It was not possible to obtain comparable values for the materials, since the available ones were for bulk materials, and in thin slices of InAs and HfO_2 higher breakdown values are expected. The obtained peak electric field through the device at $V_{\mathrm{GB}} = 0.5V, V_{\mathrm{GF}} = -0.5V$ was at $\sim 6x10^6\, {}^{V}/_{cm}$. Also, Gupta *et al.* [1] derived an expression that can help calculate the electric field of the device.

A more conventional compound used for LEDs due to its photoelectric properties and the wavelength of $0.37\mu m$ in the UV region is gallium nitride GaN. The same optimal thickness used in the case of InAs, when applied for GaN, with gate work-functions adjusted accordingly, all at thermal equilibrium, (fig. 8A) does not show any carrier concentrations in the front or back side of the semiconductor ($n_{\mathrm{i_{GaN}}} = 1x10^{10}\, cm^{-3}$). This is due to its relatively wide bandgap (3.507eV) which requires more energy to direct recombination. In this case, a reverse bias application to increase carrier concentrations is necessary, as shown in fig. 8B, and decreasing the GaN body thickness could result in improved concentrations. Even then, if the values at thermal equilibrium were to be used for GaN, the required regeneration time T would be $\sim 10^9$ seconds which is highly infeasible. A transient simulation illustrating this can be found in Appendix E.

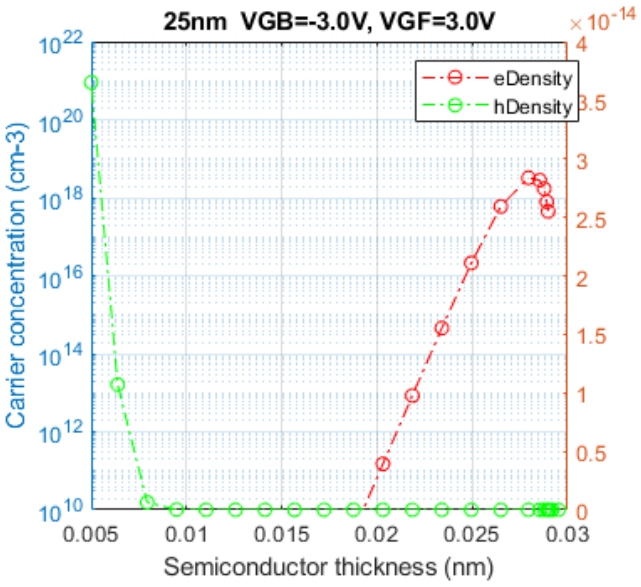

Figure 8A. Carrier concentration for GaN, with the optimal device thickness as in the case of InAs, and gate workfunctions adjusted for GaN ($\phi_{m,F} = 3.7eV, \phi_{m,B} = 5.65eV$), at thermal equilibrium.

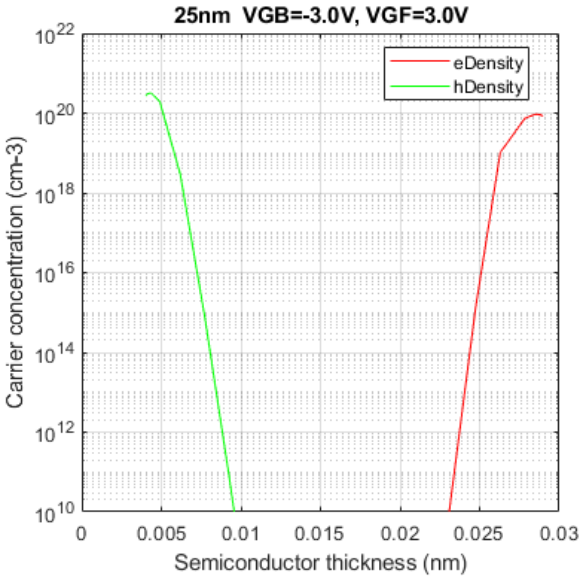

Figure 8B. Carrier concentrations for GaN with gate biases set at V_{GB} = -3.0V, V_{GT} = 3.0V, at thermal equilibrium

Another mode of operation for the EHB device is to use it as a (forward biased) p-n junction diode, by removing the oxide layers. The semiconductor thickness is 25nm and length is 500nm. In fig. 10 the IV characteristics curve for the device is plotted. As can be seen, the device is rectifying showing an I_{on}/I_{off} ratio of ~10^4. Further, it is operating below $10^{-3}A$. As for light emission, at $-0.2V$ the $R_{rad} = 4.5x10^{27}\, {cm^{-3}}/{s}$ resulting in an IQE=61.5%.

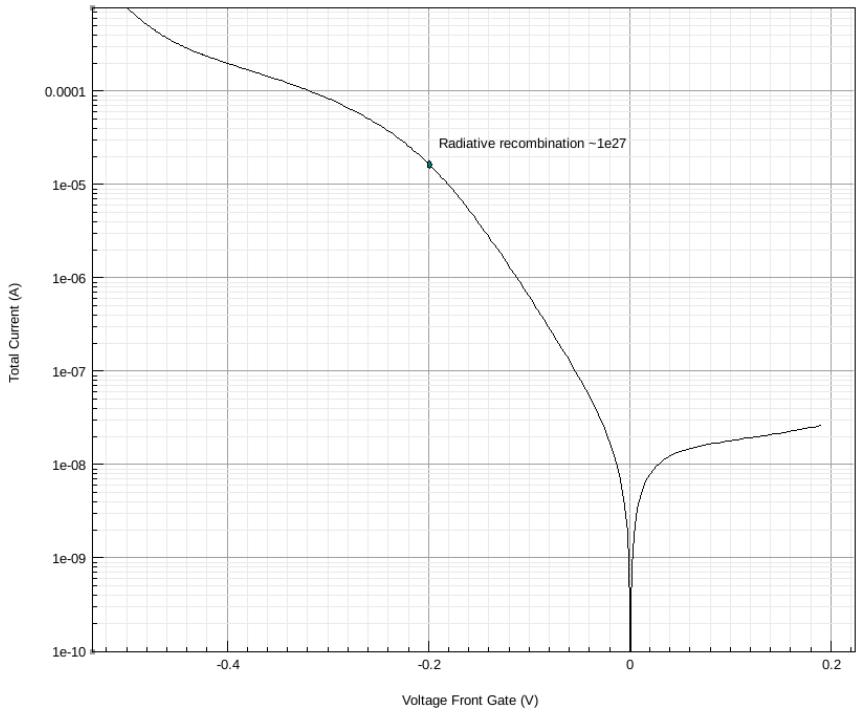

Figure 10. I-V characteristics of the device with back gate bias kept at 0V and front gate swinging between 0.5 and -0.5V

V. Conclusions

In this paper the EHB LED concept was discussed and simulated. Simulations showed that for a narrow and direct bandgap semiconductor, such as InAs, results were promising, offering high carrier concentrations at the gates, high radiative recombination rates and efficiency for the device. Due to the small size of the device, QM effects and supercoupling were a constant determining factor in the device characteristics.

The transient simulations were initially performed with a voltage swing between 0 and $\pm 0.5V$, and though the concentrations were high, and the radiative recombination as well, the SRH recombination reduced the device efficiency. When changing the voltage swing between -0.5V and 0.5V, higher concentrations were achieved and the radiative recombination surpassed the SRH resulting in a high efficiency. As discussed, these values can be highly improved if the carrier concentrations are further increased in the mentioned manners.

The effects of different device configurations were also discussed, such as altering the semiconductor thickness, changing the gate bias, and choosing different gate work-functions. Choosing a different semiconductor is also possible, however as discussed, the new device has to be configured such that there are regions of carriers formed in the semiconductor. Again, important factors to keep in mind are supercoupling, as well as the electric field. It was not possible to draw conclusions on the later due to the unavailability of comparable values.

Compared to other conventional LEDs, the EHB LED could offer improved performance in power consumption and efficiency. It is difficult however to evaluate its performance to other LEDs without a comparative approach into a selected group of devices, and that was beyond the scope of this paper. Other applications could include visible and UV light devices, tunnel FETs, as well as communication devices.

VI. Acknowledgements

I am highly indebted to both my day to day supervisor G. Gupta, and R. J. E. Hueting for their guidance and supervision, as well as for providing the necessary information regarding the project.

VII. References

[1] G. Gupta, B. Rajasekharan, and R. J. E. Hueting, "Electrostatic Doping in Semiconductor Devices," *IEEE Transactions on Electron Devices*, vol. 64, no. 8, pp. 3044–3055, 2017

[2] M. Prunnila, J. Ahopelto, "Two sub-band conductivity of Si quantum well", *Phys. E Low-Dimensional Syst. Nanostruct.*, vol. 32, no. 1, pp. 281-284, 2006.

[3] M. Prunnila, S. J. Laakso, J. M. Kivioja, J. Ahopelto, "Electrons and holes in Si quantum well: A room-temperature transport and drag resistance study", *Appl. Phys. Lett.*, vol. 93, no. 11, pp. 112113, 2008.

[4] R. J. E. Hueting, B. Rajasekharan, C. Salm, and J. Schmitz, "The charge plasma P-N diode," IEEE Electron Device Lett., vol. 29, no. 12, pp. 1367–1369, Dec. 2008.

[5] C. C. Hu, *Modern semiconductor devices for integrated circuits*. Upper Saddle River: Prentice Hall, 2010.

[6] Adachi, Properties of Group-IV, III-V and II-VI , Semiconductors,John Wiley & Sons, Ltd, 2005
[7] J.-C. Fan and S.-F. Lee, "Effect of Oxide Layer in Metal-Oxide-Semiconductor Systems," *MATEC Web of Conferences*, vol. 67, p. 06103, 2016.
[8] Sentaurus TCAD, Version l-2016.03 ed. Synopsys Inc., Mountain View, CA, USA, 2016
[9] S. Cristoloveanu, S. Athanasiou, M. Bawedin, and P. Galy, "Evidence of Supercoupling Effect in Ultrathin Silicon Layers Using a Four-Gate MOSFET," *IEEE Electron Device Letters*, vol. 38, no. 2, pp. 157–159, 2017.
[10] S. Eminente, S. Cristoloveanu, R. Clerc, A. Ohata, and G. Ghibaudo, "Ultra-thin fully-depleted SOI MOSFETs: Special charge properties and coupling effects," *Solid-State Electronics*, vol. 51, no. 2, pp. 239–244, 2007.
[11] V. Puliyankot and R. J. E. Hueting, "One-Dimensional Physical Model to Predict the Internal Quantum Efficiency of Si-Based LEDs," *IEEE Transactions on Electron Devices*, vol. 59, no. 1, pp. 26–34, 2012.
[12] "Photoelectric Work Function | The Elements Handbook at KnowledgeDoor," *KnowledgeDoor*. [Online]. Available: http://www.knowledgedoor.com/2/elements_handbook/photoelectric_work_function.html. [Accessed: 14-Dec-2018].

VIII. APPENDIX

Appendix A

Table A2. Carrier concentrations for $\phi_{m,F} = 4.82eV, \phi_{m,B} = 5.65eV, V_{GB} = 0.0V, V_{GF} = 0.0V$

$t_{SC}(nm)$	$eDensity\ (cm^{-3})$	$hDensity\ (cm^{-3})$
10	5.4654e-49	8.0824e+18
15	1.4544e+15	2.5122e+18
20	1.7988e+16	3.9387e+18
25	7.4721e+16	4.8203e+18
30	1.5922e+17	5.4214e+18
50	3.9199e+17	6.3384e+18
80	4.6206e+17	6.6122e+18

Table A3. Carrier concentrations for $\phi_{m,F} = 4.82eV, \phi_{m,B} = 5.65eV, t_{SC} = 25nm$

$V_{GB}, V_{GF}\ (V)$	$eDensity\ (cm^{-3})$	$hDensity\ (cm^{-3})$
0.0, 0.0	7.4721e+16	4.8203e+18
0.0, 0.2	6.9995e+17	3.9784e+18
0.0, 0.5	2.2307e+18	3.3505e+18
0.0, 1.0	5.4877e+18	3.4113e+18
0.0, -0.2	6.6066e+14	5.8337e+18
0.0, -0.5	1.8295e+12	6.7573e+18
0.0, -1.0	6.5297e+11	1.4517e+19
0.2, 0.0	1.3129e+17	1.7802e+17
0.5, 0.0	4.3861e+17	2.7461e+13
1.0, 0.0	1.4726e+18	2.1945e+10
-0.2, 0.0	6.9371e+16	1.4360e+19
-0.5, 0.0	7.2586e+16	3.1715e+19
-1.0, 0.0	8.7725e+16	6.7201e+19
0.2, -0.2	1.1557e+15	4.9536e+17
0.5, -0.5	1.5192e+14	3.7290e+16
1.0, -1.0	5.5535e+17	1.2066e+19
-0.2, 0.2	6.7812e+17	1.3580e+19
-0.5, 0.5	2.2039e+18	3.0616e+19
-1.0, 1.0	5.5029e+18	6.6282e+19

Highlighted values are concentrations when the gate polarity is reversed (electrons in the back and holes in the front)

Table A4. Carrier concentrations for $V_{GB} = 0.0V, V_{GF} = 0.0V, t_{SC} = 25nm$

$\phi_{m,F}, \phi_{m,B}\ (eV)$	$eDensity\ (cm^{-3})$	$hDensity\ (cm^{-3})$
4.82, 5.65	7.4721e+16	4.8203e+18
4.72, 5.75	3.0557e+17	8.7366e+18
4.92, 5.55	8.3557e+15	8.2652e+17

Appendix B

Figure B1. Simulation results for different bias configurations

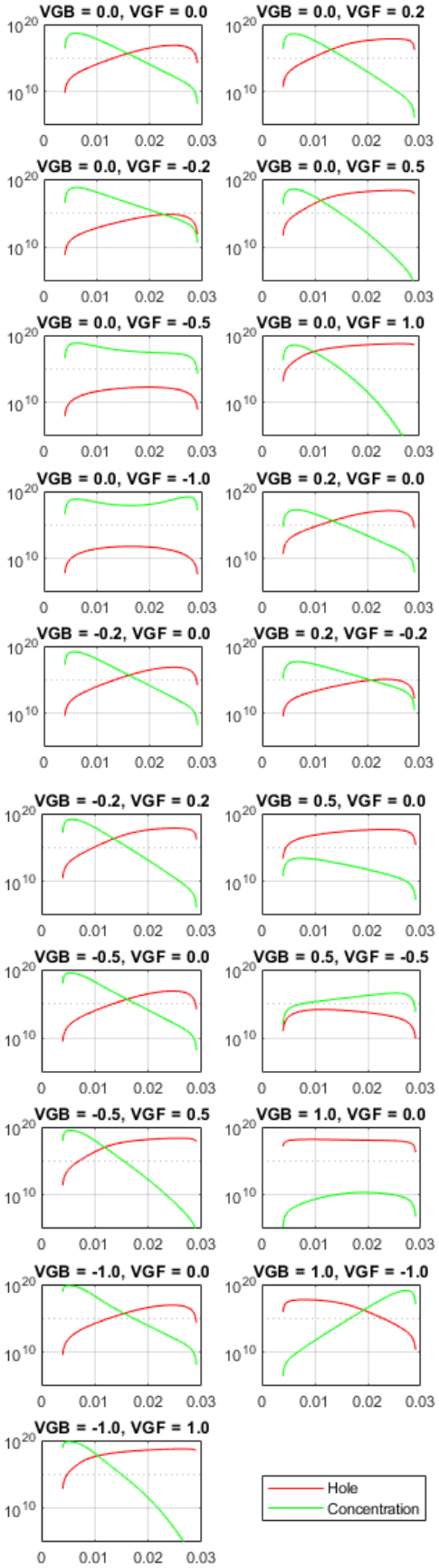

Appendix C

The following is a transcript of equations derived by R. J. E. Hueting, University of Twente.

" The question is: what parameters affect the thermal generation rate?

Some things have been explained in the book of D. Schroder; in particular p.426-427 are of interest.

Let's fist determine what is affecting the generation rate. The continuity equation tells us that:

$$\frac{dn}{dr} = G,$$

where holes are ignored.

In case of SRH generations

$$p = n = n_i e^{\left(\frac{V}{2* n_t}\right)} \; ; \; (\mathrm{V} < 0) \wedge \tau_h = \tau_p = \tau_{SRH}$$

$$G_{SRH} = \frac{p * n - n_i^2}{\tau_p * (n + n_i) + \tau_h * (p + n_i)}$$

$$= \frac{n_i(e^{\left(\frac{V}{2* n_t}\right)} - 1)}{2 * T_{SRH}} \approx -\frac{n_i}{2 * \tau_{SRH}}.$$

There is also bulk generation from Auger:

$$G_{Aug} = -\frac{n}{\tau_{Aug}} = -\frac{n_i^2}{N_A} * \frac{D_n}{L_n^2}.$$

And in case of III-V materials b2b generation:

$$G_{rad} = -\frac{n}{\tau_{rad}} = -B_{rad} * n_i^2.$$

In addition, there are lateral surface generation components as described by Schroder, ignored in this work.

So,

$$\frac{dn}{dr} = G_{SRH} + G_{rad} + G_{Aug}$$

$$= -\frac{n_i}{2 * \tau_{SRH}} - B_{rad} * n_i^2 - \frac{n_i^2}{N_A} * \frac{D_n}{L_n^2}.$$

Now, to determine the total time T to generate n_0 electrons it can be stated that:

$$n_0 = \int_0^T G \, dt = -\int_0^T \left(\frac{n_i}{2 * \tau_{SRH}} + B_{rad} * n_i^2 + \frac{n_i^2}{N_A} * \frac{D_n}{L_n^2}\right) dt$$

In principle the generation components do not have a strong time dependence. So we can therefore state:

$$T = \frac{n_0}{\frac{n_i}{2 * \tau_{SRH}} + B_{rad} * n_i^2 + \frac{n_i^2}{N_A} * \frac{D_n}{L_n^2}}$$

Conclusion: T drops exponentially for smaller bandgaps. The actual lifetimes are less important.

For the EHB concept the bulk generation can be ignored.

$$T = \frac{n_0}{\frac{n_i}{2 * \tau_{SRH}} + B_{rad} * n_i^2}$$

Considering wide-band gap materials:

$$T = \frac{n_0}{n_i} * 2 * \tau_{SRH}$$

General: Narrow band gap materials are more eligible for ED and EHB concept in particular. ”

Appendix D

Table D1. Recombination rates values for InAs transient simulations

	Radiative	Auger	SRH
0	1494150	341.9828	1.48E+09
2	118906.8	30.7268	1.16E+08
4	116479.3	32.75791	96579467
6	155391.3	43.64196	1.17E+08
8	162644.7	42.59134	1.29E+08
10	140713.2	24.40593	97735146
12	1.11E+16	0	6.09E+18
14	3.30E+17	0	3.81E+20
16	1.40E+19	0	1.19E+22
18	3.06E+20	0	1.02E+23
20	2.94E+21	0	3.13E+23
22	1.85E+17	0	1.93E+19
24	1.72E+14	0	1.80E+16
26	1.67E+11	0	1.72E+13
28	6.59E+09	14934515	4.83E+11
30	16020078	52633.4	1.26E+09
32	4.03E+20	5.31E+17	1.28E+23
34	1.63E+19	6.74E+15	1.37E+22
36	4.06E+17	1.08E+14	4.68E+20
38	2.06E+16	3.02E+12	1.13E+19
40	1.13E+17	0	1.10E+20
42	85636.88	5.683987	1.42E+08
44	27945344	2891.474	3.88E+10
46	16662832	5639.938	1.21E+10
48	17111551	5840.515	1.36E+10
50	73052.11	8.409414	81486213
52	1.11E+16	0	6.09E+18
54	3.30E+17	0	3.81E+20
56	1.40E+19	0	1.19E+22
58	3.06E+20	0	1.02E+23
60	2.94E+21	0	3.13E+23
$V_{GB} \rightarrow -0.5$		$V_{GF} \rightarrow 0.5$	
62	1.60E+22	0	5.31E+23
64	6.21E+22	0	6.56E+23
66	1.91E+23	0	6.62E+23
68	4.54E+23	0	5.44E+23
70	8.24E+23	0	3.66E+23
72	9.08E+15	0	4.12E+15
74	9.65E+10	0	5.15E+10
76	1.52E+12	4.76E+10	4.69E+11
78	8.66E+09	64519615	7.72E+09
80	9.5E+09	3.31E+08	5.75E+09

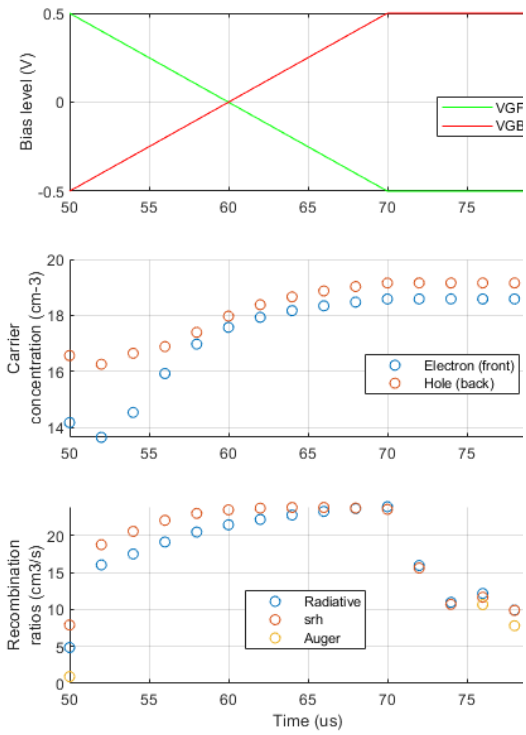

Figure 3. Remainder of the simulation in figure 6, when bias is applied to increase carrier concentrations before switching to forward.

Appendix E

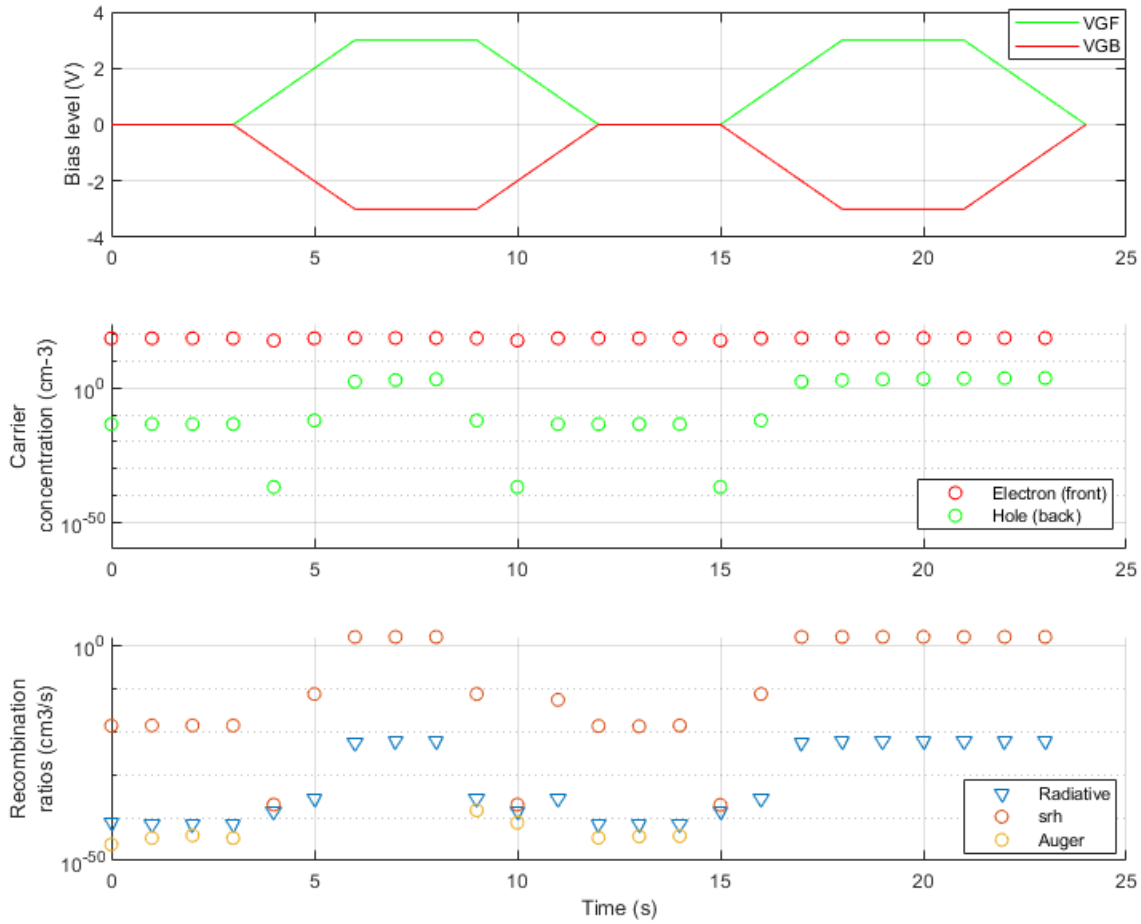

Figure D1. Transient simulations for GaN with $\phi_{m,F} = 3.7eV, \phi_{m,B} = 5.65eV$ and V_{GB} = -3.0V, V_{GT} = 3.0V. The simulation is run in seconds, and as can be seen, there is not enough time for thermal generation to complete and reach high levels of carrier concentrations. As mentioned previously, it would take a long amount of time in the case of GaN to generate enough carriers.